Liquid metal embrittlement and deformation induced martensite: The case of 316 L austenitic steel LME by liquid eutectic gallium-indium

Thierry Auger, Vincent Michel, Laurent Cassayre, H. Baketi, B. Barkia, A. Michel, E. Perrin

To cite this version:

Thierry Auger, Vincent Michel, Laurent Cassayre, H. Baketi, B. Barkia, et al.. Liquid metal embrittlement and deformation induced martensite: The case of 316 L austenitic steel LME by liquid eutectic gallium-indium. Corrosion Science, 2021, 192, pp.109850. ⟨10.1016/j.corsci.2021.109850⟩. ⟨hal-03448780⟩

HAL Id: hal-03448780
https://hal.science/hal-03448780v1

Submitted on 25 Nov 2021

Liquid metal embrittlement and deformation induced martensite: the case of 316L austenitic steel LME by liquid eutectic gallium-indium

T. Auger[1,2,**], V. Michel[1], L. Cassayre[3], H. Baketi[2], B. Barkia[2], A. Michel[2], E. Perrin[2]

[1] PIMM, Arts et Métiers Institute of Technology, CNRS, Cnam, HESAM Université, 151 boulevard de l'hôpital, 75013 Paris, France
[2] MSSMAT, Ecole CentraleSupélec, UMR CNRS 8579, Grande voie des vignes 92295 Chatenay-Malabry, France
[3] Laboratoire de Génie Chimique, Université de Toulouse, CNRS, INPT, UPS, 4, Allée Emile Monso, F-31030 Toulouse, France

Abstract:

The liquid metal embrittlement sensitivity of a low nickel 316L austenitic steel has been studied with eutectic gallium indium alloy. The embrittlement case is firmly established with this steel and studied by X-Ray fractography and EBSD. Brittle to ductile recoveries were observed via a dedicated parametric study (varying cross-head speed and temperature). The return to ductility with temperature is strongly correlated with a significant reduction in plastically induced α' phase change suggesting it is a requirement for LME. This implies a strategy focused on limiting deformation induced martensite to design LME resistant austenitic steels at low temperature.

Keywords: Stainless steels, X-ray diffraction, LME

1 Introduction

Liquid Metal Embrittlement (LME) is referred to as the reduction of elongation to fracture during a mechanical test when the material is put in intimate contact with a liquid metal. LME of austenitic steels is rarely mentioned in the literature, aside from the well-known case of an austenitic steel embrittled in contact with zinc at high temperature because it is presumed to be a potential step in the disastrous failure of a pipe at the Flixborough chemical plant in UK in 1972 [1]. A few other occurrences have been reported at intermediate temperature in alkali liquid metals. AISI 304L steel was found to have an intergranular LME fracture mode in liquid sodium and liquid lithium at lower temperature (between 200°C and 400°C) with moderate to limited mechanical degradation [2, 3, 4]. Similar intergranular cracking of the 304 austenitic steel was also noticed during tertiary creep in sodium at 550°C [5]. LME is also observed at ambient temperature but with a subset only of the commonly studied austenitic steels in low melting point liquid media such as mercury or gallium [6, 7, 8].

---

[*] Corresponding author : thierry.auger@ensam.eu, Laboratoire PIMM, Arts et Métiers Paristech-CNRS-CNAM, UMR CNRS 8006, 151 Bd de l'Hôpital 75013 Paris
Tel: 33 (0) 1 71 93 65 21

Screening LME tests carried out by Krupowitz indicate that 304, 304L and 321 austenitic steels are embrittled in liquid mercury while on the contrary, the 316 and 316L steels used in this study are not [6]. In apparent contradiction with the previous study, a low nickel version of 316L was found to be sensitive to LME with mercury [8]. Similarly, a nitrogen added low nickel 316LN steel was found to be affected by mercury during oligocyclic fatigue tests at room temperature but not at the higher temperatures reached at high frequency tests [9]. At last, using a fracture mechanics compact tension (CT) geometry, the 316L steel of the study was found to be weakly embrittled by Ga (of the order of 15% reduction in fracture toughness) [7]. These tests were carried out at two temperatures only (35 to 75°C). On the other hand, post-exposure tests of 316L in contact with Ga showed only a slight reduction in the total ductility at room temperature [10].

Understanding the spread in material's sensitivity is the starting point of this work. It is not yet clear what triggers LME sensitivity of austenitic steels with low melting point liquid metals (gallium or mercury) at near room temperatures. It is however interesting to note that it concerns essentially the low nickel nuances (at least in the works where the steel composition is explicitly given such as [7]). One could advocate that the LME sensitivity seems dependent upon the steel's chemical composition and the related austenite stability (the low nickel metastable austenitic steels display a γ to α' phase transformation upon plastic deformation). The link about fracture along γ/α' interfaces created during plastic deformation is actually the conclusion reached in a study of 304L in contact with liquid sodium [11,12]. One also unfortunately notes unreported experimental details about the essential wettability criterium in mechanical testing in several works casting doubts in the case of negative conclusion [7, 10]. The essential question in this works was whether or not an intimate contact was obtained between the steel and the liquid metal. There is also the matter of whether or not the strain rate or temperature range of testing was adequate because LME can be sometimes only observed in a limited strain rate and temperature range [10]. Due to the lack of extensive testing, it has been difficult up to now to come up with a clear understanding for the occurrence of LME around room temperature in the case of austenitic steels. The present paper is an attempt to fill this gap in the case of a low nickel 316L austenitic steel embrittled with the liquid eutectic gallium-indium (eGaIn).

We first carried out a strain rate dependence sensitivity study to set the strain rate range where LME can be observed. Then a study of the temperature dependence of LME was carried out between the room temperature and 110°C, precisely in the range where α' phase transform strongly depends upon temperature with a complete disappearance in the upper range. Local analysis by Electron Backscattered Diffraction (EBSD) and X-ray fractography were carried out to assess the fracture path and the amount of phase changes as a function of the kinetic parameter (testing strain rate and temperature). X-ray fractography allows to probe the phase fraction in metastable austenitic steels immediately beneath the fracture surface with a penetration depth not exceeding a few µm [13]. Initially used for phase transformation studies of fatigue samples, this technique is used here in a novel way to probe for phase transformations in fracture. This allowed us to clearly establish for the first time the correlation between LME induced fracture and the α' phase transformation trend showed by the alloy used here. This conclusion enlightens the spread in the LME sensitivity found in the literature. It also suggests a potential road for suppressing low temperature LME sensitivity with austenitic steels.

2 Experimental procedure

2.1 Materials

The composition of the 316L steel is reported in table 1. The Md_{30} (the temperature at which tensile straining to 30% induces 50 vol.% of martensite) is equal to -54°C according to the Nohara correlation [14]. The mean intercept grain size was 30 µm. The material was in an annealed and quenched metallurgical state. The chemical metallurgy of austenitic steels was further characterized (chemical micro-segregation of delivered products, stability of the austenite phase with δ-ferrite formation in area with low amount of nickel). The content of δ-ferrite was quantified by X Ray diffraction using its (110) diffraction peak compared with the (111) diffraction peak of γ-austenite. The content of δ-ferrite was found to be of 0.8% ± 0.4%. The phase was evidenced by optical microscopy as thin strips parallel to the rolling direction. The chemical micro-segregation of the sheet was characterized by the Lichtenegger and Bloech I color etching technique. Micro-segregation bands of nickel in the rolling direction were found similar to what is usually found [15,16]. This indicates a potential chemical heterogeneity of the material at a scale of the order of hundreds of µm. Energy Dispersive Spectroscopy (EDS) semi-quantitative mapping was carried out on mirror polished samples and the chemical heterogeneity was confirmed with a clear variation in the nickel content (at the % level). Given the influence of the nickel content on the martensitic transformation, it is expected to lead to spatial heterogeneities in the phase transformation distribution.

The choice of the liquid metal is driven by practical considerations. We wished to have it liquid already at ambient temperature as well as, for convenience, with limited concerns with vapor spread when heated. Unlike mercury, gallium and indium have extraordinarily low vapor pressures even at upper range of investigated temperatures (at 373K, $P°(Hg)=3.10^{-4}$ atm, $P°(Ga)=2.10^{-32}$ atm, $P°(In)=7.10^{-29}$ atm [**17**]) that renders both handling and use very easy in a mechanical tensile test chamber. High purity gallium (99.999%) and indium (99.9995%) were procured from Alfa Aesar. A melt with the eutectic composition (Ga-15at%In) was formed by dissolving the appropriate amount of indium in liquid gallium just above its melting point temperature. According to the Ga-In phase diagram, the solidus temperature is 15°C at the eutectic composition.

2.2 Chemistry of eGaIn in diluted hydrochloric solutions and wettability

In order to establish the embrittlement case, it is necessary to ensure a direct contact between the gallium-indium liquid phase and the 316L steel surface. For this purpose, we developed a chemical etching procedure, aiming at simultaneously avoid oxide scale formation on the gallium-indium eutectic and dissolve the native chromium oxide on the austenitic steel. Provided these two conditions are met, the liquid metal spreads on the metallic surface with a near zero wetting angle signaling an almost total wetting of the steel by eGaIn. The important steps in the wetting procedure are sketched in Fig. 2a.

Such a chemical etching process was already successfully applied with mercury on 316L steel in a 4% HCl aqueous solution with long exposure (several hours) [18]. There is however a significantly different chemical behavior between mercury and gallium-indium in hydrochloric acid solution. The former is inert while the later strongly reacts with water with a visible gas release. The Eh-pH diagram of indium and gallium in an aqueous media containing chloride ions was computed with the help of the FactSage software combined with FactPS database [17]. As illustrated in Fig. 1, these two metals are not stable in water and tend to oxidize, forming gaseous hydrogen and an oxidation product. The nature of the oxidation product is either a solid oxide compound or a soluble ion, depending on the acidity of the solution. For instance, in the case of Ga:

For pH > 1.25 $2Ga_{(s)} + 3H_2O \longrightarrow Ga_2O_{3(s)} + 3H_{2(g)}$

For pH < 1.25 $2Ga_{(s)} + 6H^+_{(aq)} \longrightarrow 2Ga^{3+}_{(aq)} + 3H_{2(g)}$

Similarly, indium dissolves as In^{3+} ions at low pH and forms a solid In_2O_3 oxide phase at higher pH, with a pH threshold of about 2.6. Even if the values of these pH thresholds depend on the metal/water ratio, this general behavior is valid within a large concentration range.

Figure 1: Superposition of Ga, In and Cr Eh-pH diagrams at 25°C (molarity of metals is 0.1 mol.kg^{-1}; molarity of Cl^- is 0.5 mol.kg^{-1}).

The Ga-In eutectic has roughly the same pH-dependent behavior as its pure components: above a threshold pH, an oxide phase (either pure Ga_2O_3 or a mixture of Ga_2O_3 and In_2O_3) forms at the liquid eutectic - water interface. This would prevent wetting by forming an interfacial oxide entirely covering the interface. Below this pH threshold, the interface remains oxide free and the liquid metal is continuously consumed as gallium and indium ions, associated with dihydrogen release. As also shown in Fig. 1, chromium oxide dissolves into $CrCl_2^+$ at pH below 3.75, so that conditions adapted for Ga-In eutectic etching will also be convenient to remove the typical passive chromium oxide layer of an austenitic steel.

A study of the wetting pre-treatment was carried out to find the optimal conditions in terms of hydrochloric acid concentration. Mirror polished flat pieces of 316L austenitic steels were exposed to a drop of eGaIn under varying concentration of hydrochloric acid. The optimal concentration was set at 10 weight% ([HCl]=3.18 mol/L ; pH=-0.5), a condition well below the pH threshold required to avoid oxide formation on eGaIn. This ensured that Ga-In quickly spreads on the flat steel's surface while limiting the dihydrogen release rate. With flat samples and at this concentration, spreading with a small wetting angle over a square centimeter occurs within a few minutes.
A transverse cut by ionic beam was tried for Scanning Electron Microscopy (SEM)-EDS analysis to look for potential interfacial phases that would have formed upon the wetting treatment. Unfortunately, it proved difficult to perform adequately as the liquid film would migrate upon cutting and would make EDX analysis meaningless because the liquid film usually covers the interfacial area.

The pre-wetting treatment in the case of 316L with eGaIn has a potential drawback. Dihydrogen is produced copiously at the interface, possibly leading to hydrogen uptake by the steel. It was therefore deemed necessary to analyze any potential role on the embrittlement of the steel of the dihydrogen produced using such a process. It could happen that if embrittlement is observed then it would not be necessarily due to the liquid metal but to hydrogen embrittlement. In order to evaluate if this scenario is a potential source for embrittlement in our case, one can estimate the characteristic length for hydrogen diffusion ($l = \sqrt{2Dt}$) for the time interval comprising pre-wetting and testing. The typical time scale for pre-wetting is less than one hour with an exposure time of a quarter of an hour. After drying, carrying to the tensile test apparatus, mounting and testing, no more than two hours has elapsed. The diffusion coefficient D in $m^2.s^{-1}$ for H_2 in 316L austenitic steel is given by the following equation [19].

$$D = 6.2 \times 10^{-7} \exp\left(-\frac{53630}{RT}\right)$$

where R is the ideal gas constant ($J.K^{-1}.mol^{-1}$) and T is the temperature in Kelvin. At room temperature (T=293K), the diffusion coefficient D_{RT} reads $1.68x10^{-16}$ $m^2.s^{-1}$. This gives for the characteristic length for hydrogen diffusion in a typical experiment (overall three hours at most) a value of roughly 2 µm ($l = \sqrt{2Dt}$). The mechanical effect of an affected layer over such a characteristic diffusion length would be very low and, in any case, will be neglected. Additional tensile testing carried out after the pre-wetting treatment followed by removal of the liquid gallium-indium film did not show any sign of embrittlement.

2.3 Mechanical testing

Axisymetric notched tensile specimens were machined from the as-received material in the transverse direction. The gauge diameter was 4 mm, the gauge length was 15 mm. A notch of 600 µm depth was machined with a tip radius of 100 ± 5 µm for the set to be tested at room temperature and a tip radius of 40 ± 5 µm for the set to be tested above.

The tensile specimen notch was exposed to the 10 weight% hydrochloric solution to chemically etch the native oxide. While still under the cover of the acidic solution, a small drop of eGaIn melt was inserted into the notch using a variable volume pipette. The melt immediately reacts with the acidic solution releasing dihydrogen. After a typical time of a few minutes during which a few rotations along the longitudinal axis are manually performed, the eGaIn wets and fills the notch thereby providing a reservoir that will supply liquid eGaIn to the propagating crack tip. The excess hydrochloric solution is wiped out using dry paper thereby stopping further dihydrogen release.

The eGaIn wetted specimens were tested at room temperature (slightly above 20°C) as a function of the cross-head speed using an electro-mechanical uniaxial loading machine (MTS 20/M). The cross-head speed tested covers three orders of magnitude from $8.33x10^{-8}$ $m.s^{-1}$ to $8.33x10^{-5}$ $m.s^{-1}$. A reference specimen was systematically tested without eGaIn for comparison for every cross-head speed. Due to the notched geometry, the mechanical measurements (load, cross-head displacement) are not normalized. Instead the test results are analyzed using the energy to fracture (J) calculated by integrating out the load-displacement curve. The degree of embrittlement is measured by the ratio between the energy to fracture in eGaIn normalized by the reference energy to fracture (J/J_{ref}). The main error source associated with this procedure stems from the sample to sample fluctuation in notch depth (conservatively taken to be 10 µm at most). The estimated error is then of the order of 3%. An embrittling condition is revealed when this ratio is well below unity.

The mechanical tests carried out above the room temperature (from 35°C to 200°C) were performed at a testing speed of $8.33x10^{-7}$ $m.s^{-1}$ (this will be seen to correspond to the speed of maximal embrittlement at room temperature). A reference specimen was also systematically tested without eGaIn for comparison for each temperature. The Joule effect heating technique was used with a low voltage high current flowing through the sample. The temperature was measured and regulated using a 1 mm diameter type K thermocouple inserted at the notch location. To avoid oxidation issues during these tests, the materials were tested under a high purity Ar cover gas (dioxygen and water impurity levels are continuously kept lower than 1 weight ppm).

2.4 Microstructural characterization

After mechanical testing, the fracture surface is covered with a liquid film of gallium-indium. In order to remove this film and perform the SEM analysis, ultrasonic cleaning in distilled water of the broken specimen for a few minutes was tested as can be done with mercury [18]. However, even if this procedure efficiently removed most of the liquid metal, a solid interfacial film of significant thickness remains. This film contains Ga and In according to EDX point spectrum of the sample surface. We concluded that a part of eGaIn remains or forms interfacial intermetallics in contact with the steel surface and cannot be removed by this technique.

This procedure is nevertheless very useful to check whether the sample was wetted correctly before testing. Indeed, un-wetted area due to air or dihydrogen bubbles would prevent the liquid metal to reach the tip of the notch as it can be seen on Figure 2b. A rapid scan of the samples tested in eGain showed that there was at most a few of these spots preventing direct contact with the liquid phase. It indicates that the mechanical tests were carried out with a proper initial wetting state because the influence of the few unwetted areas is deemed negligible.

Figure 2: a) Sketch of the wetting process (sequence starting at the top). b) Crack initiation site showing a sparse spot of unwetted area (Test temperature 50°C, cross-head speed of 8.33×10^{-7} m.s^{-1}). The dashed line outlines the crack front.

Another procedure was thus applied to prepare the set of broken samples in eGaIn for the fractographic analysis of the fracture surface. The fractured part was dug into mercury for less than one hour to amalgamate the gallium-indium remaining film, thanks to the large solubility of gallium and indium in liquid mercury at room temperature. This amounts at using mercury as a solvent for gallium and indium. The eGaIn liquid film is replaced by a mercury rich film with dissolved traces of gallium and indium. The sample is then wiped out of its mercury cover by ultrasonic cleaning in distilled water as achieved in a previous work [18]. The fracture surface is then free of liquid eGaIn but the interfacial phase is only partially removed preventing a correct analysis by X-ray fractography. This preparation technique was therefore complemented by an anodic attack in diluted soda (0.1 mol/l concentration, PH = 13) at 1 V during 15 minutes for the samples initially covered by liquid eGaIn. This procedure is a slightly simplified form of the technique already used by Kolman et al. which is known not to affect the steel's surface [7]. It was checked that the procedure allowed to completely remove the liquid metal and the interfacial phase without affecting the steel's surface.

The fractographic analysis was carried out in a FEG-SEM (FEI Helios 650). The microstructural analysis of the plastically deformed area was carried out by Electron BackScattered Diffraction (EBSD) on radial transverse cuts obtained by ion beam polishing (Jeol CrossPolisher). The 1 mm wide ion beam cuts were located at the notch location and included the crack initiation site as well as a fraction of the crack propagation zone. The EBSD mapping was carried out such as to cover an area near the fracture surface up to a depth and length of several hundred micrometers. In order to maximize the significance of the orientation mapping and phase determination, a high electron beam current was systematically used (6 nA) and sixteen EBSD patterns were superposed on each point allowing to reach high image quality and very high orientation confidence index. Step sizes of 0.1 or 0.15 µm were used. Two phases (cfc austenite and cc ferrite phases) were allowed in the EBSD pattern fit procedure to detect the initial material and a potential α' phase transformation.

The X-ray fractography was conducted on a PANalytical X'Pert diffractometer equipped with a Philips PW3040 X Ray generator and a X'Celerator real time multiple strip detector. A tube with a copper anode was used emitting mainly through the K_α ray at a wavelength of 0.15416 nm (run at a high voltage of 45 kV with a current of 40 mA). The 2θ diffraction data were collected from 30° up to 100° with a step of 0.037° with an integrated acquisition time of 50 s. Fixed anti-scatter and divergence slits of 0.04 rad were used together with a beam mask of 10mm and all scans were carried out in the so-called continuous mode. The resultant collimated beam size was of the order of 1 mm at the level of the sample (full width at half maximum).

Phase identification was carried out by means of the High Score Plus software (from PANalytical) using the Crystallography Open Database (Version january 2020) [20,21]. The quantification was pursued using the integrated intensities of all the diffraction peaks from each of the identified phases, the cfc austenitic phase (COD Reference code: 96-900-8470 modified with the correct cell parameter for 316L [22]) and the bcc ferritic phase (COD Reference code: 96-900-8537, it is to be noted that the α' phase of the austenitic steel has a cell parameter almost identical to pure iron [23]). In spite of the differing height of the diffracting areas of a rough fracture surface, the angular separations between the peaks used for this semi-quantitative analysis are sufficient to allow for an accurate quantification. A Rietveld quantification was also carried out with one spectrum that yielded results within one percent so the semi-quantitative approach was pursued for the entire set of data (the typical error by these methodologies is taken to be around 3% [24]).

Additionally, a X-ray diffraction spectrum was obtained from the machined surface of the notch located next to the fracture surface. The quantification results showed that machining of the notch generated a significant amount of α' phase transformation at the notch's side surface (56% of α' phase compared with 0.8% initial). To avoid this unwanted contribution to X-ray fractography, it was therefore deemed necessary to mask the inner machined notch surface during acquisition. A polysiloxane film of 200 µm thickness was prepared by polymerization that is known to give only a diffuse ordering contribution in diffraction [25]. The thickness was set after an absorption assessment of the X-ray beam by searching for the extinction of diffraction peaks of an austenitic steel substrate covered by the film. A hole of 2mm diameter was punched in a square cut of the silicone (1x1 cm^2) and the film was fixed in place to cover most of the notch leaving only the fracture surface exposed to X-rays at the hole location. This film hence prevents unwanted diffraction from the notch side at the expanse of adding an amorphous background that is easily subtracted in the quantitative analysis.

All the fracture surfaces, both from the reference samples fractured in argon and the samples fractured by eGaIn were scanned by X-ray fractography. The latter set of samples, being fully cleared of the remnant of the undesirable interfacial Fe-Ga phase, were therefore probed for the relative α' and γ phase fraction in search for potential LME induced changes in the phase transform evolution with deformation.

3 Results

3.1 Mechanical tests

Typical load-displacement curves are shown in Figure 3 for a test carried out in contact with liquid eGaIn at room temperature at a cross-head speed of 3.33x10^{-7} m.s^{-1} together with its reference. In these conditions, the data indicate a clear lowering of the mechanical properties in contact with eGaIn. The maximum load is lowered compared to the reference curve and the displacement to rupture is decreased. The data shown are close to the most damaging condition found in this study.

Figure 3: Load versus cross-head displacement graph at room temperature of 316L austenitic steel reference and tested in eGaIn (cross-head speed of 3.33x10^{-7} m.s^{-1}).

The results of the tests at room temperature for cross-head speed from 8.33x10^{-8} m.s^{-1} to 8.33x10^{-5} m.s^{-1} are summarized in Figure 4 using the ratio of the energy to fracture (J/J_{ref}). One can see that there is maximum embrittlement at low cross-head speed (a drop from 35 to 38% of the energy to fracture). There is a ductility recovery between 10^{-6} and 10^{-5} m.s^{-1} cross-head speed till a complete ductile recovery at higher speed with nearly identical energy to fracture for both conditions (wetted and reference).

Figure 4: Degree of embrittlement vs cross-head speed at room temperature.

Based on these data, a cross-head speed of 8.33x10^{-7} m.s^{-1} was selected for the tests to be carried out as a function of temperature. One mechanical test with eGaIn along with one reference test were performed for each temperature between 35°C and 110°C. The same analysis using the ratio of the energy to fracture is carried out for the parametric study as a function of temperature (Figure 5). At temperatures slightly above room temperature up to 50°C, the mechanical effect of eGaIn is embrittling (a drop from 38% to 26% of the energy to fracture). From 62°C and up to the highest tested temperature (200°C), an almost complete ductile recovery is observed. Therefore, within a little more than 10°C temperature interval, a drastic change of fracture mode occurs with a transition from a brittle cracking mode to a ductile mode.

Figure 5: Degree of embrittlement vs temperature (8.33x10^{-7} m.s^{-1} cross-head speed).

3.2 Fractography

Fractographic analysis reveals that, at designated embrittling cross-head speed and temperatures conditions, brittle crack initiation takes place at the tip of the notch giving an outer ring of brittle fracture surface (Figure 6a from a test carried out at 35°C and 8.33x10^{-7} m.s^{-1}). The brittle area extends over several hundred's µm deep towards the center (see Figure 6b) then the fracture surface appearance switches to large and elongated cupules. The final cracking has a ductile like aspect that can be explained by the strain rate acceleration beyond necking at the end of the test recalling that a ductility recovery is observed as the cross-head speed is increased past a threshold cross-head speed of 10^{-5} m.s^{-1}.

Figure 6: 316L-eGaIn tested at 35°C and 8.33x10^{-7} m.s^{-1}. a) low magnification of the fracture surface and b) general view of the crack initiation site on the left of a).

At high magnification, the fracture surface in the brittle area (Figure 7) has a “quasi-cleavage” fracture surface type with numerous steps and crack branching sites that do not seem correlated with the initial austenitic microstructure.

Figure 7: High magnification view of the fracture surface for 316L-eGaIn tested at 35°C and 8.33×10^{-7} m.s^{-1}.

From the fractographic examination of the specimen tested at the highest cross-head speed with eGaIn (Figures 8a and 8b), one finds that the fracture surface is fully ductile with no sign of brittle cracking even at high magnification as expected from the ductility recovery observed mechanically. A detailed examination over the entire crack initiation ring showed that there is not a single brittle crack initiation site.

Figure 8: 316L-eGaIn tested at room T° and 8.33×10^{-5} m.s^{-1}. a) low magnification of the fracture surface and b) close view of the crack initiation site on the left of a).

From the fractographic analysis of the sample tested at 62°C and a cross-head speed of 8.33×10^{-7} m.s^{-1} in eGaIn (Figures 9), one finds that the fracture surface has a ductile appearance with no sign of brittle cracking away from the notch area. This confirms the ductility recovery measured via the mechanical properties. However numerous brittle crack initiation sites can be observed within a depth of 10 µm at most from the tip of the machined notch. These evidences of brittle crack initiation are located in the specimen part that could have been affected by machining and have a significant initial deformation.

Figure 9: Close view of the crack initiation for 316L-eGaIn tested at 62°C and 8.33×10^{-7} m.s^{-1}.

3.3 EBSD analysis on transverse cuts

EBSD mapping on transverse cuts was carried out for the samples tested at different crosshead speeds at room temperature. The maps are located in the vicinity of the notch or up to the fracture surface and allow to characterize both the local orientation and phase structure. A typical EBSD map for an embritling condition (room temperature and 8.33×10^{-7} m.s^{-1} cross-head speed) is shown in Figure 10a as well as the corresponding phase map (Figure 10b) obtained by superposing the image quality indicator (IQ) and the color code for the two phases (γ in white and α' in red). Misorientation line profiles reveal numerous twin boundaries formed during plastic deformation (60° misorientation). These boundaries are visible in prior austenitic steel grains as grey lines of IQ contrast revealing heavily twinned microstructure. At room temperature, one also observes a significant fraction of the mapped area in the α' phase at all cross-head speeds. At 8.33×10^{-7} m.s^{-1} cross-head speed, a fraction of 18% of the initial austenite phase has transformed to α' while it increases up to 28% at 8.33×10^{-5} m.s^{-1} cross-head speed. Given the limited area available for EBSD analysis and given the fact that the notch of the sample induces a localized but heterogeneous plastic deformation, the phase transformed fraction is only indicative and a statistical significance cannot be reliably estimated therefore only the raw numbers are given here for a qualitative discussion.

Figure 10: EBSD mapping of a transverse cut below fracture surface of 316L fractured in GaIn at room temperature and 8.33x10^{-7} m.s^{-1} cross-head speed a) crystalline orientation + IQ b) phase map + IQ (α' in red)

EBSD mapping was carried out on the samples from 35°C to 75°C. Increasing the temperature while keeping the same cross-head speed results in a different outcome. Whereas mechanical twinning is still observed by EBSD up to a temperature of 75°C without visible pattern change, phase transform from γ to α' is observed to decrease from 18% at ambient temperature, 12% at 50°C, to roughly 7% at 75°C (See EBSD Figures 11 and 12).

Figure 11: EBSD mapping of a transverse cut below fracture surface of 316L fractured in eGaIn at a temperature of 50°C and 8.33x10^{-7} m.s^{-1} cross-head speed a) crystalline orientation + IQ b) phase map + IQ (α' in red)

Therefore, qualitatively, as the temperature is increased, the fraction of α' transformed material strongly decrease. The change from brittle fracture at room temperature to an almost fully ductile fracture at 75°C is therefore clearly correlated with the drop in the amount of material undergoing α' transformation during plastic deformation. Interestingly, on the sample tested at 75°C, the transverse cut was carried out in one of the few brittle areas at the notch (a brittle ring of 10 µm is also seen at 62°C). A locally high fraction of α' transformed material was found below this brittle fractured zone (most likely stemming from prior plastic deformation imprinted during machining).

Figure 12: EBSD mapping of a transverse cut below fracture surface of 316L fractured in eGaIn at a temperature of 75°C and 8.33x10^{-7} m.s^{-1} cross-head speed a) crystalline orientation + IQ b) phase map + IQ (α' in red)

3.4 X-ray fractographic analysis on fracture surfaces

The X-ray fractographic spectra were analyzed by removing the background which was fitted by a polynomial covering the angular range [35°-100°]. Typical spectra with the background subtracted are presented in Figure 13 for a sample fractured at room temperature and at 60°C. One observes that the (111) peak from the γ phase is well separated from the (110) peak of the α' phase for quantitative analysis.

Figure 13: X-ray θ-2θ background subtracted spectrum of the fracture surface of the 316L steel (ambient T° and 60°C)

The semi-quantification results are presented in the Figures 14 and 15 as a function of temperature and cross-head speed. The results for both the reference tests and the tests carried out in GaIn are included for discussion.

Figure 14: X-ray Fractography semi-quantification function of temperature

The α' phase fraction up to fracture has a strong variation in the range of investigated temperature. As expected, the 316L steel of this study is highly unstable relative to the martensitic transformation up to fracture at room temperature (71% of transformed α' for reference samples) while as temperature increases the martensitic transform is less and less favored (complete to almost complete disappearance at 200°C). This is consistent with the known behavior of austenitic steels where the driving force for the martensitic transforms decreases with temperature [26]. An indicative temperature for the 50% fraction threshold after 30% deformation level (Md_{30}) of -54°C is obtained using the Nohara correlation [14]. Here the higher deformation reached at fracture explains the higher fraction of transformation. A spike on the α' phase fraction can be observed at 83°C for the reference state. This is unexplained and one can hypothesize that it could result from a deviation in the local steel's composition or from some sample to sample variations. On the other hand, the evolution for the α' phase fraction with temperature is very regular for the tests in eGaIn with a drop from 63% down to undetectable at the highest tested temperature.

Figure 15: X-ray Fractography semi-quantification function of cross-head speed

For the tests as a function of cross-head speed, the α' phase fraction for the reference samples shows a small dependence upon loading rate with a slight trend towards decreasing fraction with an increase in loading rate until one reaches a limiting fraction at higher cross-head speed. For the samples fractured in GaIn, a decrease in α' phase fraction is also observed in the low rate domain with increasing cross-head speed then a sudden jump to higher fraction is observed (correlated with the brittle-ductile transition speed). One can rationalize this increase by noticing that the strain up to fracture above the transition is then systematically higher than in the embrittling domain such that an increase in the α' phase fraction stems from the higher deformed state. These variations are however small and a clear trend is less discernable than when varying temperature.

4 Discussion

The embrittlement by liquid eGaIn of a 316L austenitic steel was studied as a function of cross-head speed at room temperature and as a function of temperature at a selected constant cross-head speed. Adequate wetting pre-conditioning is ensured via a chemical etching preparation in 10 wt% HCl solution. The thermodynamics analysis using factSage of the relative stability of gallium, indium and chromium oxides as a function of pH shows that these oxides are not stable in this acidic solution. Therefore, the observed enhanced wettability is understood as stemming from the fact that a direct contact (oxide free contact) is obtained between the steel and the liquid alloy. The near zero wetting angle indicates that the austenitic steel/eGaIn couple is a system showing total wetting, i.e. that the solid-liquid interface energy is lowered by a large amount compared with the initial steel's surface energy. The need to remove a micron thick layer after mechanical testing hints at the existence of binary or ternary phases that forms at room temperature at the solid-liquid interface. It is therefore likely that the wetting behavior of the system relates to the classes of reactive wetting, i.e. wetting on an in-situ formed intermetallic compound (the phase diagram has a room temperature phase $FeGa_3$ [27]).

From the parametric mechanical study, a first important finding is that a LME sensitivity is observed at room temperature in the lower range of the investigated cross-head speeds. There is a ductility recovery at cross-head speeds comprised between 10^{-6} to 10^{-5} $m.s^{-1}$. The use of a tensile notched specimen allows to give a quantitative estimate of the degree of embrittlement based on an energetic approach (energy to fracture). In our geometry, the reduction of the energy to fracture is found to be of the order of 30% as compared with 15% in the study of Kolman using a CT geometry in contact with gallium [7]. There can be various origins for such a difference: it could possibly be an effect of indium addition, a change due to the differing steel composition or an effect of the test geometry. Nevertheless, the order of magnitude of the embrittlement (a moderate embrittlement) is similar, therefore the LME case already observed on 316L steel with gallium [7] has been reproduced here albeit with an eutectic gallium-indium melt.

When varying the temperature from room temperature to 200°C, a clear transition from brittle to ductile fracture is also observed above 50°C. Therefore, as commonly observed with LME, there is a well-defined kinetic parameters range where it can be observed (here low strain rate and low temperature). There exist therefore two recovery transitions with a return to a ductile fracture mode, a strain rate controlled one and a temperature controlled one.

Among the possible explanations for brittle to ductile recovery, one can think that it could either be material's related or an intrinsic feature of the LME mechanism. One can readily rule out the effect of a concurrent phase formation at the solid/liquid interface. Such a process should rather hinder LME at low cross-head speed (LME would then be observable only at high speed). The opposite dependence is seen here in our parameter range. Therefore, a scenario of a concurrent phase formation hindering LME does not fit with the data reported here.

The brittle to ductile transition occurs while α' phase transformation induced by plastic deformation or Deformation Induced Martensite (DIM) is observed at a high level throughout all the investigated cross-head speed range as evidenced by EBSD and most importantly quantified by X-ray fractography (around 70% with a low at 57%). Therefore, the transition in fracture mode is weakly correlated with a change in the material plastic deformation mode. Indeed, the strain-rate dependence of DIM formation requires several orders of magnitude higher strain rates than used in this study to see a significant drop of the DIM fraction in austenitic steels. This effect is believed to be due to the adiabatic heating during plastic deformation [28]. The transition cross-head rate here (between 10^{-6} and 10^{-5} $m.s^{-1}$, see Figure 4) is however too low for adiabatic heating to change the test temperature significantly. The observed brittle to ductile transition as a function of strain rate instead hints at the existence of a rate-limiting process inherent to the LME crack propagation phenomenon itself. Such limiting crack propagation rate related to the desorption kinetics was observed in another work with a steel in contact with eutectic PbBi [29]. Another possibility is that it could be related to intergranular penetration kinetics with a maximum crack propagation rate yet to be explained. The recovery mechanism as a function of testing speed is therefore still to be clarified.

The brittle to ductile recovery as a function of temperature, on the contrary, is strongly linked with the termination of the DIM domain with increasing temperature. The EBSD analysis shows clearly a drop in the fraction of α' phase transformation as the test temperature is increased from room temperature to 75°C where LME is no longer observed. Similarly, the more accurate data from the X-ray fractography show a drop from 65-70% of DIM down to zero at the highest temperature studied here (200°C). Most of the drop occurs also within a small temperature range (between 50 to 60°C). This is seen for the reference data but also for the samples tested in eGaIn. The behavior of our 316L steel follows closely the expected temperature dependence of DIM formation of austenitic steels as modelled recently by Das et al. [30]. Based on a compilation of data on similar austenitic steels (composition wise), the mean fraction of DIM formation is expected to decrease from 0.4 to 0.1 at 125°C (it is to be noted that the DIM formation is largely strain rate independent [30]). One can represent the correlation between the degree of embrittlement (taken as $1\text{-}J/J_{ref}$) and the measured fraction of α' phase (Figure 16). On can see a very good correlation between the two parameters using the data for samples fractured in GaIn. A Spearman's correlation test gives a p value of 0.0067 for embrittlement not being correlated to DIM fraction (selecting data around the transition temperature up to 110°C). This test is used to probe the likelihood of the correlation coming from a random fluctuation in the case of non-gaussian distributed variables (as opposed to the classical Pearson correlation test). The degree of embrittlement is therefore found here to be highly correlated with the measured fraction of α' phase for the temperature variation.

Figure 16: Correlation between degree of embrittlement and α' phase fraction for Gain tested samples with varying temperatures [RT,110°C]

In a recent detailed study down to the nanoscale of the crack path of a LME case of a 304L austenitic steel [11], it was concluded that α' phase transformation also plays a key role in providing a mechanism by which interfaces produced during plastic deformation are then later embrittled by the liquid metal. The observed arrested interfacial cracks are evidence that the crack follows an interfacial pathway and that the quasi-cleavage aspect of the fracture surface reflects rather an extremely complex interfacial crack path in a plastically fragmented microstructure [11]. The orientation mapping analysis carried out at small scale with the 304L steel showed that a significant fraction of the analyzed area underwent α' phase transformation and deformation induced interfaces are clearly formed here at room temperature. Shear-band or shear-band grain boundary intersections or grain boundary triple point were found as potential nucleation sites for α' phase transformation [31].

This is confirmed in the case studied in this work by the analysis by X-ray fractography that finds a large fraction of transformed steel when LME is observed. A large density of interfaces is then formed in the steel that can readily be embrittled by eGaIn. It is likely that the crack path in our case is also intergranular per se. Further investigations would be needed at lower scales to properly characterize the crack path in this microstructure and confirm this point. It is known that bcc steels can be embrittled by liquid gallium (with an intergranular fracture induced by liquid eGaIn) [32]. At this stage, one can only speculate whether α'/γ interfaces as well can be fractured by liquid eGaIn.

One can further hypothesize that below a critical threshold of DIM, further brittle interfacial crack propagation via DIM affected sites cannot be sustained (even in the case of a completely brittle crack initiation as witnessed at 62°C, see Figure 9). Indeed, the critical site-percolation threshold for randomly packed sphere for example is known to be 0.31 giving a critical volume fraction of 0.18 [33], a value reached at a temperature slightly above 75°C on average with the mean fraction of DIM formation of austenitic steels [20]. Therefore, one may draw a scenario for the sudden recovery between 50 and 62°C. The brittle crack propagation, most likely intergranular, would then be unsustainable due to the lack of new interfaces (with the hypothesis that both α'/γ or α'/α' interfaces are embrittled) formed during plastic deformation as the DIM formation process is no longer activated. One notes that numerous twinning still takes place at all temperatures even as high as 75°C (Figure 12). These special interfaces do not seem to play a role in the fracture process here.

Overall one can derive from this work that plastic deformation induced α' phase change seems to be a necessary requirement for LME sensitivity (albeit not sufficient if another phenomenon is to be considered such as a rate limiting process for crack propagation). It is to be noted that Kolman et al. [7] mention that they did not found strain induced martensite in their study but the experimental technique is not reported. They however noticed a similar trend of increasing embrittlement as the strain rate is decreased but could not conclude for an effect of temperature. The correlation seen between plastic deformation induced α' phase change and LME is interesting regarding the phenomenology of the LME sensitivity of austenitic steels in liquid mercury. Krupowitz et al. [6] observed a sensitivity to LME that seemed correlated with the trend of the steel to undergo α' phase transformation. Indeed, the austenitic steels that were tested were either unstable or stable austenite regarding DIM formation due to varying nickel content. Interestingly, only the most unstable austenitic steels (low nickel ones) were found sensitive to LME which would indicates a similar mechanism in the steel/mercury system. This point will be checked in a forthcoming study as this would constitute a path forward to conceive materials immune to LME.

5 Conclusion

The LME sensitivity of a low nickel austenitic steel has been studied with liquid eutectic GaIn. The liquid metal induced brittle cracking at low cross-head speed found in this work confirms prior results found with liquid Ga alone [7]. A dedicated parametric strain rate study at room temperature found a brittle to ductile recovery above a threshold cross-head speed of 10^{-5} $m.s^{-1}$. A study with temperature finds a threshold temperature of 50°C above which ductility returns. While the strain rate transition is uncorrelated with α' phase change induced by plastic deformation, the temperature transition observed is on the opposite clearly correlated with the termination of plastically induced α' phase change. The Spearman statistical test for correlation gives a p value less than 0.0067 for it being the result of a statistical fluctuation. Overall, this indicates that the existence of the α' phase transformation is a necessary but not sufficient condition for LME to occur within the austenitic steel/eGaIn system. By extension, our study enlightens the low temperature LME mechanism with austenitic steels where deformation induced martensite plays a key role in the fracture process. As a consequence, it suggests that a subset of 316L steels (those stable upon deformation induced martensite) could be insensitive to low temperature LME in eutectic GaIn. It possibly also applies to other liquid metal environments as well.

Acknowledgements

The help of Sokona Konate with samples preparation for EBSD is gratefully acknowledged. The Helios 650 work was carried out using the equipment of the MATMECA consortium partially funded by the ANR under contract number ANR-10-EQUIPEX-37. Professor Emmanuel Richaud is warmly thanked for his help for providing amorphous polysiloxane masks for X rays. Jingwei Zhang is thanked for help for Rx samples preparation during her internship.

Data availability

The raw/processed data required to reproduce these findings cannot be shared at this time due to technical or time limitations.

6 References

[1] M. Andréani, P. Azou, P. Bastien, Action du zinc liquide sur les aciers au nickel, C. R. Acad. SC. Paris 263 (1966) 1041-1043
[2] V.V. Popovich, M.S. Goikhman, E.I. Polyakov, M.I. Chaevskii, The effect of lithium on the mechanical characteristics of austenitic stainless steels, Sov. Mater. Sci. 5 (1969) 345-351
[3] H.U. Borgstedt, M. Grundmann, The fracture of austenitic and martensitic steel in liquid lithium, Nuclear Engineering and Design/Fusion 3 (1986) 273-286
[4] S. Hémery, T. Auger, J.L. Courouau, F. Balbaud-Célérier, Liquid metal embrittlement of an austenitic stainless steel in liquid sodium, Corrosion Science 83 (2014) 1–5
[5] H.U. Borgstedt, H. Huthmann, Influence of sodium on the creep-rupture stainless steel, Journal of Nuclear Materials 183 (1991) 127-136
[6] J.J. Krupowicz, Effect of Heat Treatment on liquid metal-induced cracking of austenitic alloys, in: ASTM STP 1210, Slow Strain Rate Testing for the evaluation of environmentally induced cracking : research and engineering applications, R.D. Kane (Eds.), Philadelphia, 1993,pp. 193-201
[7] D.G. Kolman, R. Chavarria, Liquid metal embrittlement of type 316L stainless steel by gallium as measured by elasto-plastic fracture mechanics, Corrosion 60 (2004) 254-261
[8] L. Medina-Almazan, T. Auger, D. Gorse, Liquid metal embrittlement of an austenitic 316L type and a ferritic–martensitic T91 type steel by mercury, Journal of Nuclear Materials 376 (2008) 312–316
[9] H. Tian P.K. Liaw, D.E. Fielden, L. Jiang, B. Yang, C.R. Brooks, M.D. Brotherton, H. Wang, J.P. Strizak, and L.K. Mansur, Effects of frequency on fatigue behavior of type 316 low-carbon, nitrogen-added stainless steel in air and mercury for the spallation neutron source, Metallurgical and materials transactions A, 37A (2006) 163-173
[10] K. A. Narh, V. P. Dwivedi, J. M. Grow, A. Stana, W.-Y. Shih, The effect of liquid gallium on the strengths of stainless steel and thermoplastics, Journal of Materials Science 33 (1998) 329-337
[11] B. Barkia, T. Auger, J.L. Courouau, J. Bourgon, Multiscale investigation of crack path and microstructural changes during liquid metal embrittlement of 304L austenitic steel in liquid sodium, Corrosion Science, 127 (2017) 213-221
[12] B. Barkia, T. Auger, J.L. Courouau, J. Bourgon, Wetting by liquid sodium and fracture path analysis of sodium induced embrittlement of 304L stainless steel, J. Mater. Res., 33 (2018) 121-129
[13] K. Rajanna, B. Pathiraj and B. H. Kolster, X-ray fractography studies on austenitic stainless steels, Engineering Fracture Mechanics 54 (1996) 155-166
[14] K. Nohara, Y. Ono, N. Ohashi, Composition and grain size dependencies of strain-induced martensitic transformation in metastable austenitic stainless steels, Journal of ISIJ 63 (1977) 212-222
[15] J. Man, I.Kubena, M. Smaga, O. Man, A. Järvenpää, A. Weidner, Z. Chlup, J. Polak, Microstructural changes during deformation of AISI 300 grade austenitic stainless steels: Impact of chemical heterogeneity, Procedia Structural integrity 2 (2016) 2299–2306
[16] C. Celadaa, I. Toda-Caraballob, B. Kimb, D. San Martína, Chemical banding revealed by chemical etching in a cold-rolled metastable stainless steel, Materials Characterization 84 (2013) 142 – 152
[17] C.W. Bale, E. Bélisle, P. Chartrand, S.A. Decterov, G. Eriksson, A.E. Gheribi, K. Hack, I-H. Jung, Y-B Kang, J. Melançon, A.D. Pelton, S. Petersen, C. Robelin, J. Sangster, P. Spencer, M-A

Van Ende, FactSage thermochemical software and databases, 2010–2016, Calphad 54 (2016) 35-53.
[18] L. Medina-Almazan, J.-C. Rouchaud, T. Auger, D. Gorse, Optimization of contact conditions between iron base alloys and mercury at room temperature, Journal of Nuclear Materials 375 (2008) 102–112
[19] A. M. Brass and J. Chêne, Hydrogen uptake in 316L stainless steel. Consequences on the tensile properties, Corrosion Science 48 (2006) 3222–3242
[20] S. Grazulis, D. Chateigner, R.T. Downs, A. T. Yokochi, M. Quiros, L. Lutterotti, E. Manakova, J. Butkus, P. Moeck & A. Le Bail, Crystallography Open Database - an open-access collection of crystal structures, J. Appl. Cryst. 42 (2009) 726-729
[21] R.T. Downs, M. Hall-Wallace, The American Mineralogist crystal structure database, American Mineralogist, 88 (2003) 247-250
[22] T.S. Hummelshøj, T.L. Christiansen, M. A.J. Somers, Lattice expansion of carbon-stabilized expanded austenite, Scripta Materialia 63 (2010) 761–763
[23] J.F. Breedis, W.D .Robertson, The martensitic transformation in single crystals of iron-chromium-nickel alloys, Acta Metal. 10 (1962) 1077-1088
[24] ASTM E975-13, Standard Practice for X-Ray Determination of Retained Austenite in Steel with Near Random Crystallographic Orientation, ASTM International, West Conshohocken, PA, 2013, www.astm.org
[25] H. H. Sutherland, Z. Ali-adib, B. Gasgous, G. Nestor, An X-ray diffraction study of liquid crystal polysiloxane copolymers, Mol. Cryst. Liq. Cryst. 155 (1988) 327-336
[26] C.M. Wayman, H.K.D.H. Bhadeshia, (1996) “Phase Transformations, Nondiffusive” in: Cahn, R.W. and Haasen, P. (Eds.). Physical Metallurgy. Fourth edition. Elsevier Science Publishers, Amsterdam, The Netherlands, pp. 1507-1554
[27] H. Okamoto, The Fe-Ga (iron-gallium) system, Bulletin of Alloy Phase Diagrams, 11 (1990) 576-581
[28] J. Talonen, P. Nenonen, G. Pape, H. Hänninen, Effect of strain rate on the strain-induced $\gamma \rightarrow \alpha'$-martensite transformation and mechanical properties of austenitic stainless steels, Metallurgical and materials transactions A 36 (2005) 421-432
[29] Z. Hadjem-Hamouche, T. Auger, I. Guillot, Temperature effect in the maximum propagation rate of a liquid metal filled crack: The T91 martensitic steel/Lead–Bismuth Eutectic system, Corrosion Science 51 (2009) 2580–2587
[30] A. Das, S. Tarafder, P. C. Chakraborti, Estimation of deformation induced martensite in austenitic stainless steels, Materials Science and Engineering A, 529 (2011) 9–20
[31] A. Das and S. Tarafder, Experimental investigation on martensitic transformation and fracture morphologies of austenitic stainless steel, International Journal of Plasticity, 25 (2009) 2222-2247
[32] D.G Kolman and R. Chavarria, Liquid-Metal Embrittlement of 7075 Aluminum and 4340 Steel Compact Tension Specimens by Gallium, Journal of Testing and Evaluation, 30 (2002) 452-456
[33] M.J. Powell, Site percolation in randomly packed spheres, Phys. Rev. B, 20 (1979) 4194-4198

Element	**C**	**Mn**	**Si**	**P**	**S**	**Cr**	**Mo**	**Ni**	**Al**	**Cu**	**V**	**N**	**Ti**	**Fe**
wt%	0.0185	1.81	0.67	0.032	0.0035	16.73	2.05	9.97	0.0183	0.23	0.07	0.029	0.0058	Bal.

Table 1: composition of the 316L steel used in this study (in wt%).

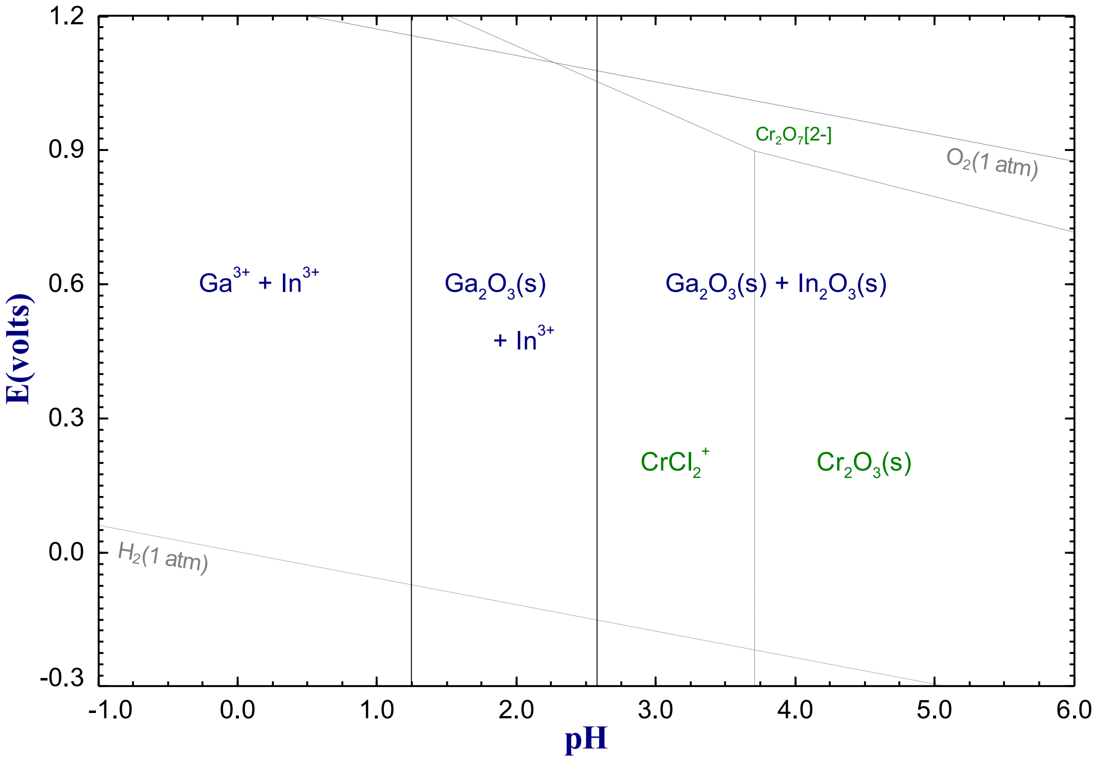

Figure 1: Superposition of Ga, In and Cr Eh-pH diagrams at 25°C (molarity of metals is 0.1 mol.kg^{-1}; molarity of Cl^- is 0.5 mol.kg^{-1}).

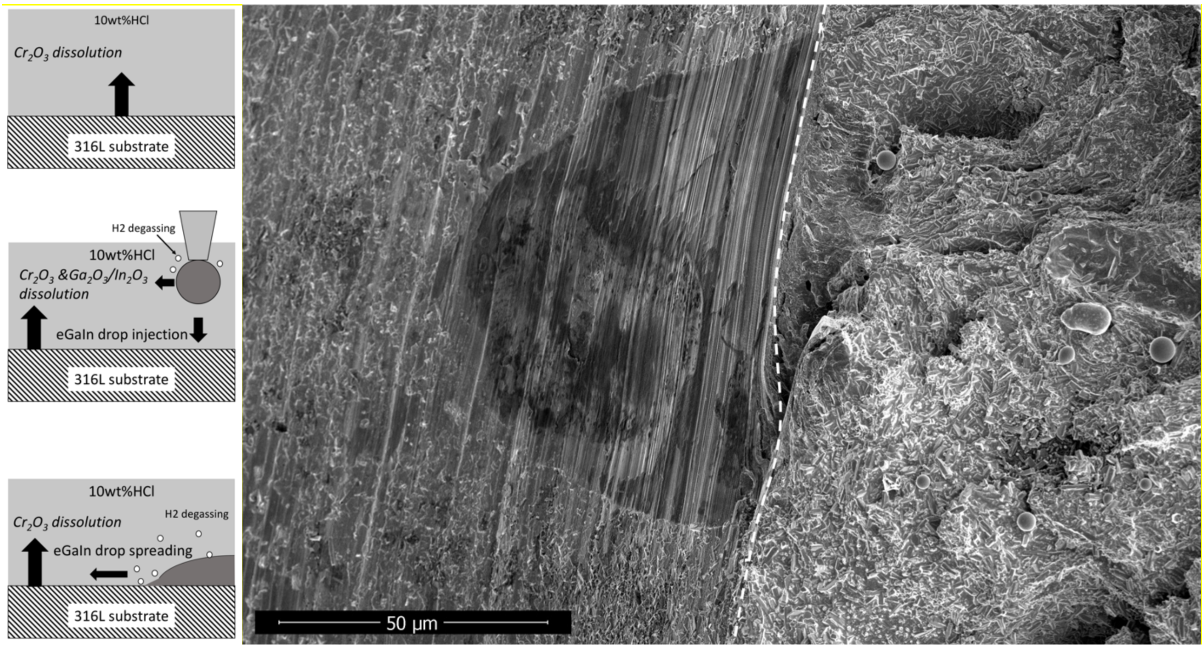

Figure 2: a) Sketch of the wetting process (sequence starting at the top). b) Crack initiation site showing a sparse spot of unwetted area (Test temperature 50°C, cross-head speed of 8.33x10^{-7} m.s^{-1}). The dashed line outlines the crack front.

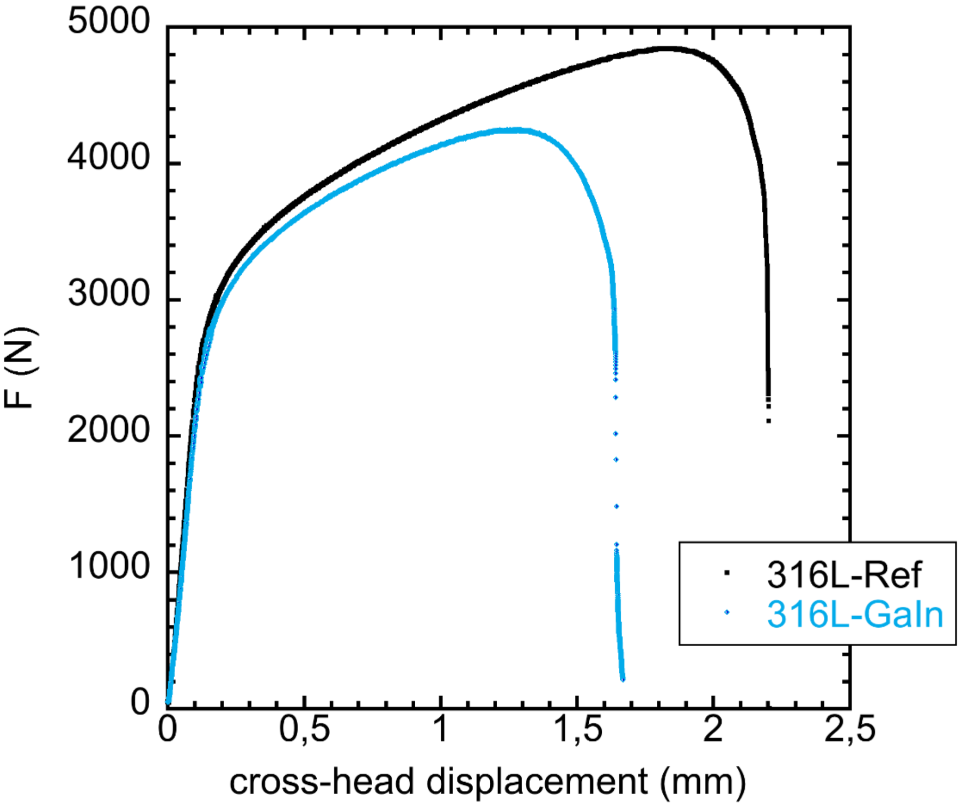

Figure 3: Load versus cross-head displacement graph at room temperature of 316L austenitic steel reference and tested in eGaIn (cross-head speed of 3.33x10^{-7} m.s^{-1}).

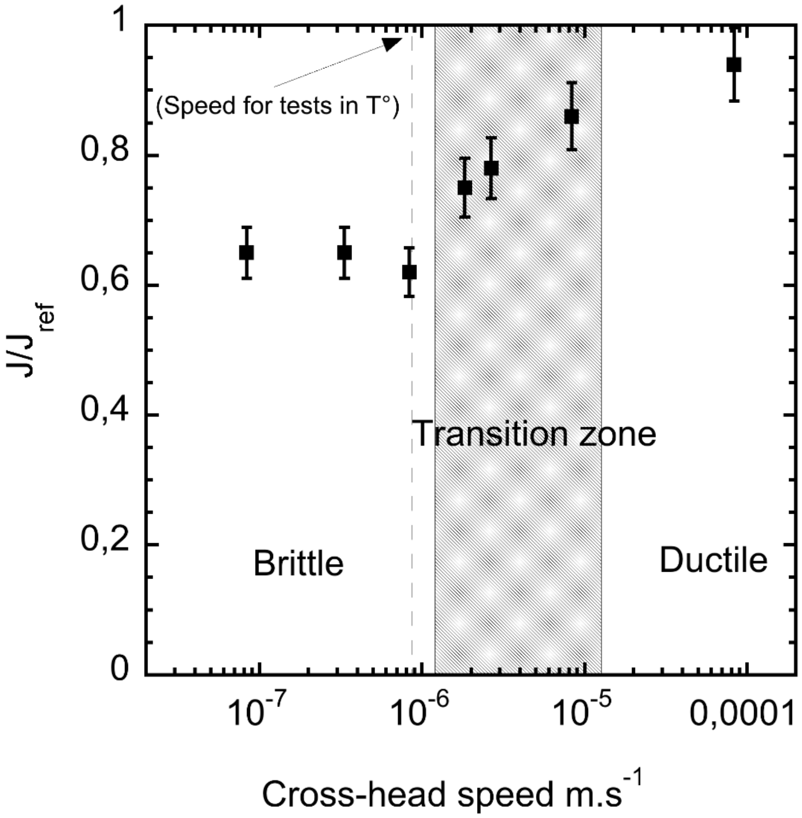

Figure 4: Degree of embrittlement vs cross-head speed at room temperature.

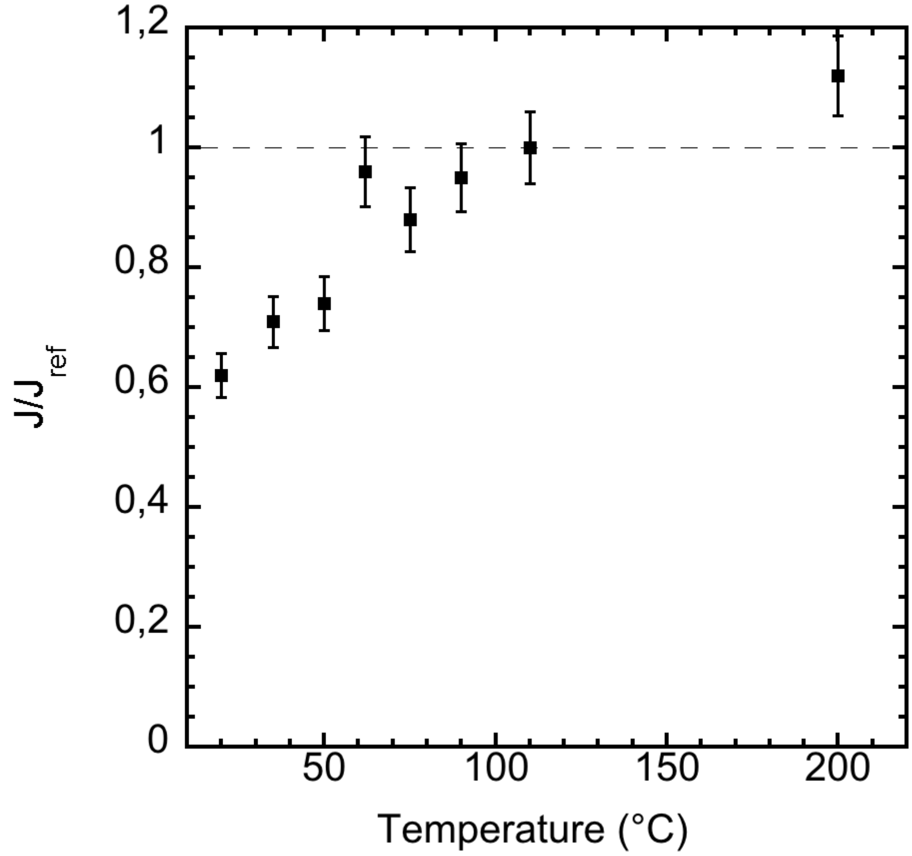

Figure 5: Degree of embrittlement vs temperature (8.33x10^{-7} m.s^{-1} cross-head speed).

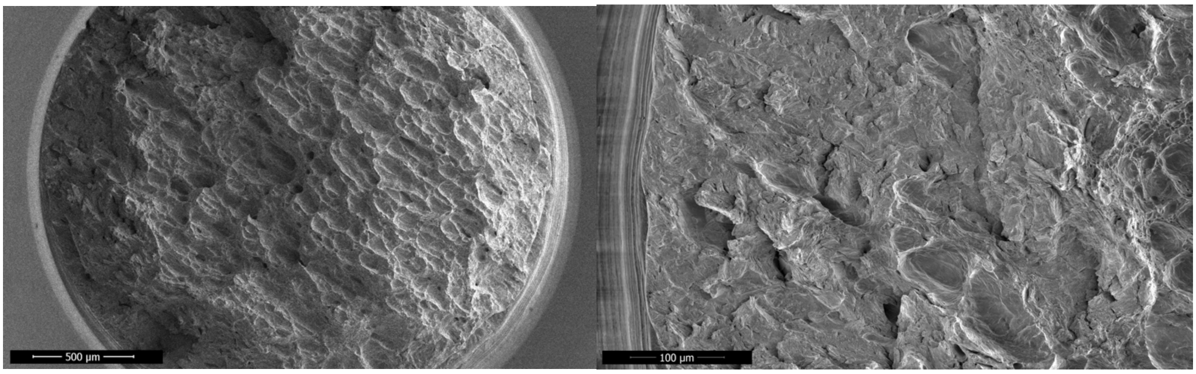

a) b)

Figure 6: 316L-eGaIn tested at 35°C and 8.33x10^{-7} m.s^{-1}. a) low magnification of the fracture surface and b) General view of the crack initiation site on the left of a).

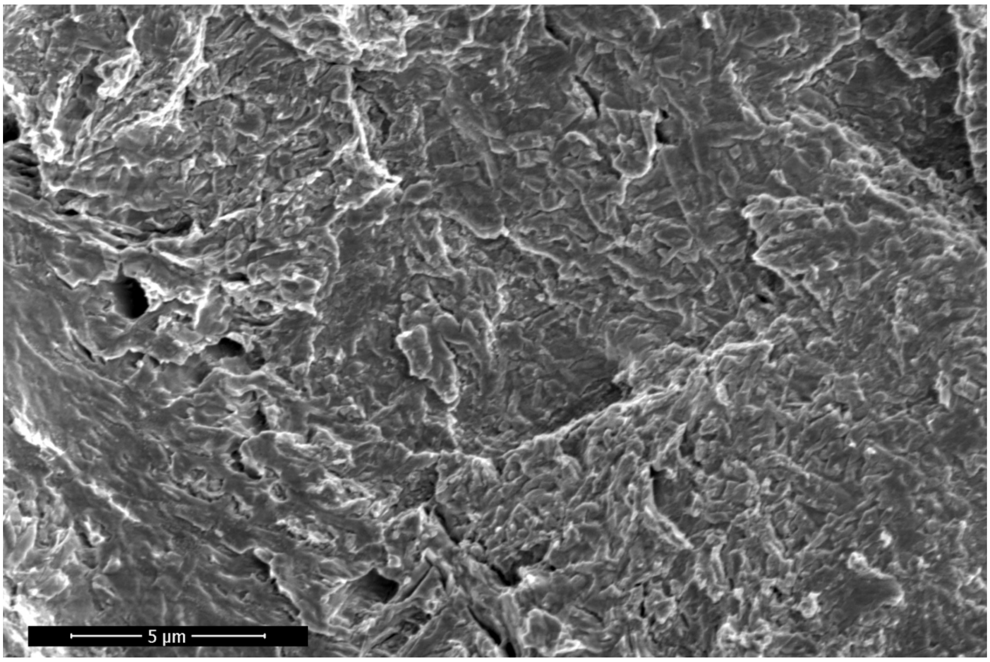

Figure 7: High magnification view of the fracture surface for 316L-eGaIn tested at 35°C and 8.33×10^{-7} m.s^{-1}.

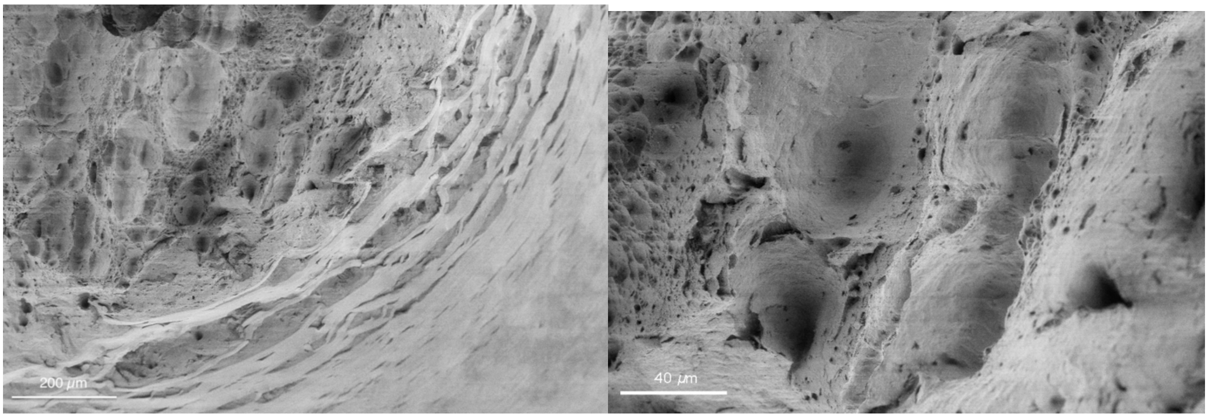

a) b)

Figure 8: 316L-eGaIn tested at room T° and 8.33×10^{-5} m.s^{-1}. a) low magnification of the fracture surface and b) close view of the crack initiation site on the left of a).

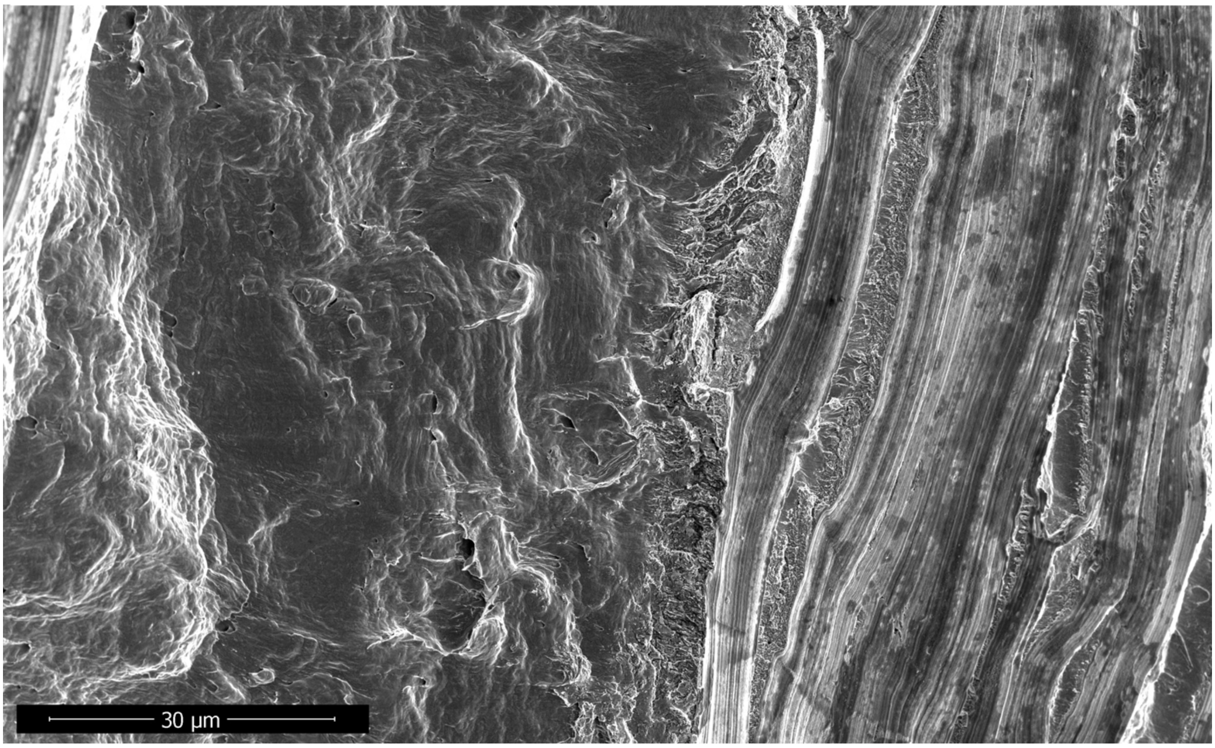

Figure 9: Close view of the crack initiation for 316L-eGaIn tested at 62°C and $8.33\text{x}10^{-7}$ m.s^{-1}.

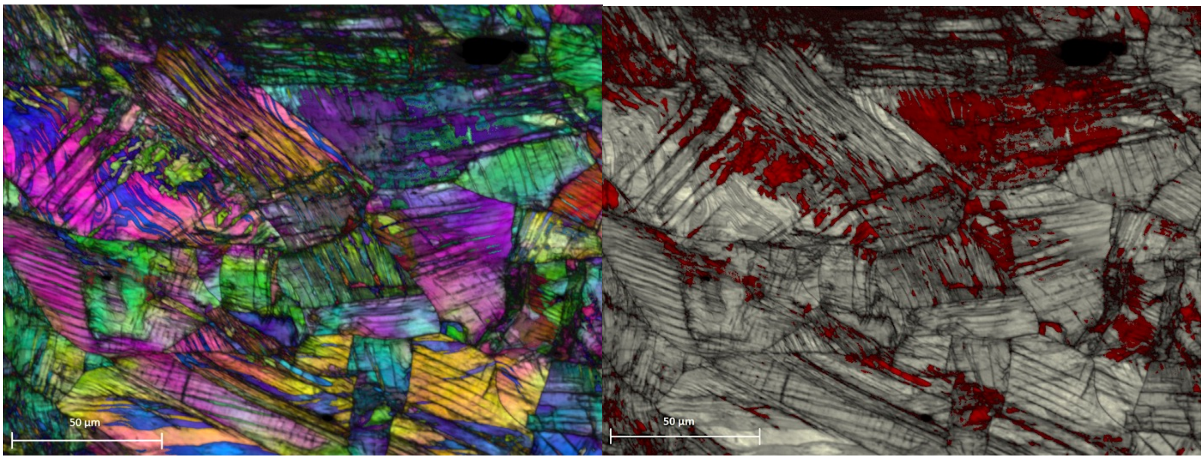

a) b)

Figure 10: EBSD mapping of a transverse cut below fracture surface of 316L fractured in eGaIn at room temperature and $8.33\text{x}10^{-7}$ m.s^{-1} cross-head speed a) crystalline orientation + IQ b) phase map + IQ (α' in red)

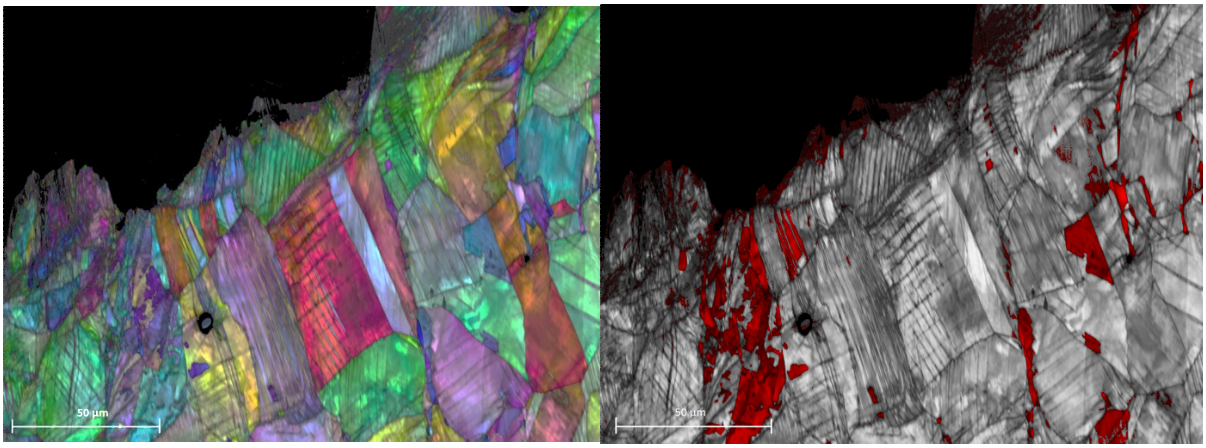

a) b)

Figure 11: EBSD mapping of a transverse cut below fracture surface of 316L fractured in eGaIn at a temperature of 50°C and 8.33×10^{-7} $m.s^{-1}$ cross-head speed a) crystalline orientation + IQ b) phase map + IQ (α' in red)

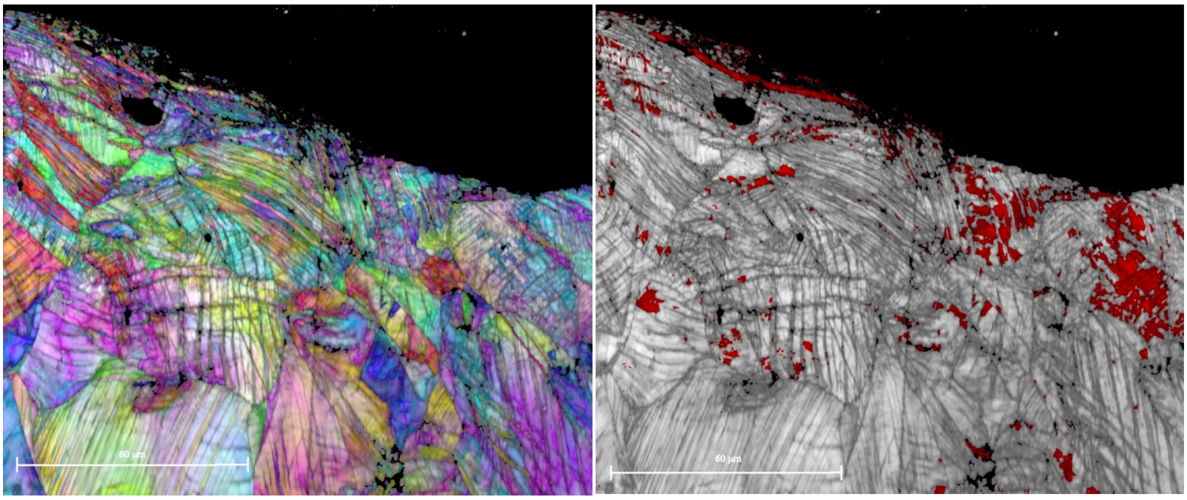

a) b)

Figure 12: EBSD mapping of a transverse cut below fracture surface of 316L fractured in eGaIn at a temperature of 75°C and 8.33×10^{-7} $m.s^{-1}$ cross-head speed a) crystalline orientation + IQ b) phase map + IQ (α' in red)

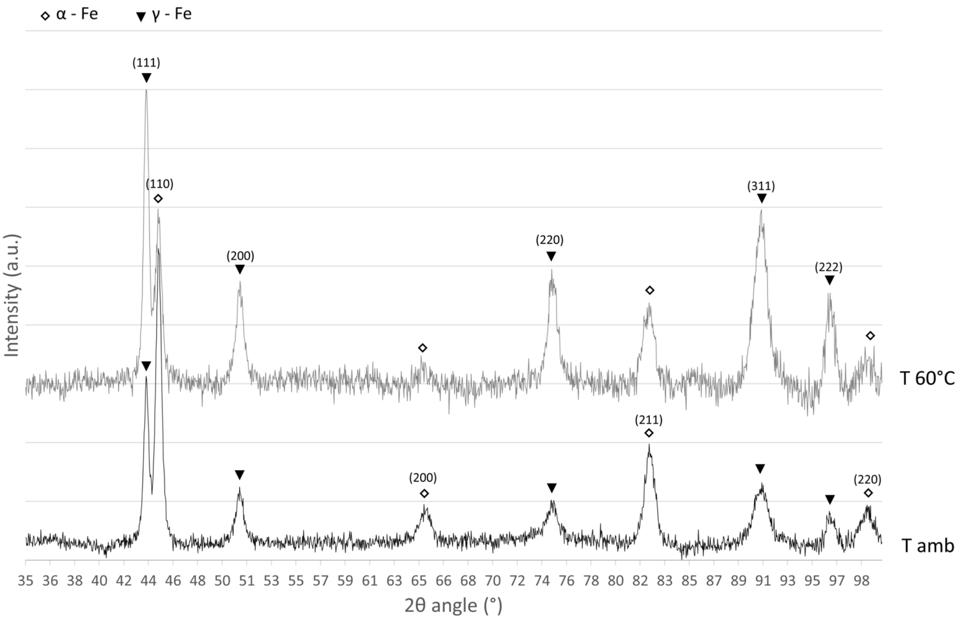

Figure 13: X-ray θ-2θ background subtracted spectra of the fracture surface of the 316L steel (ambient T° and 60°C)

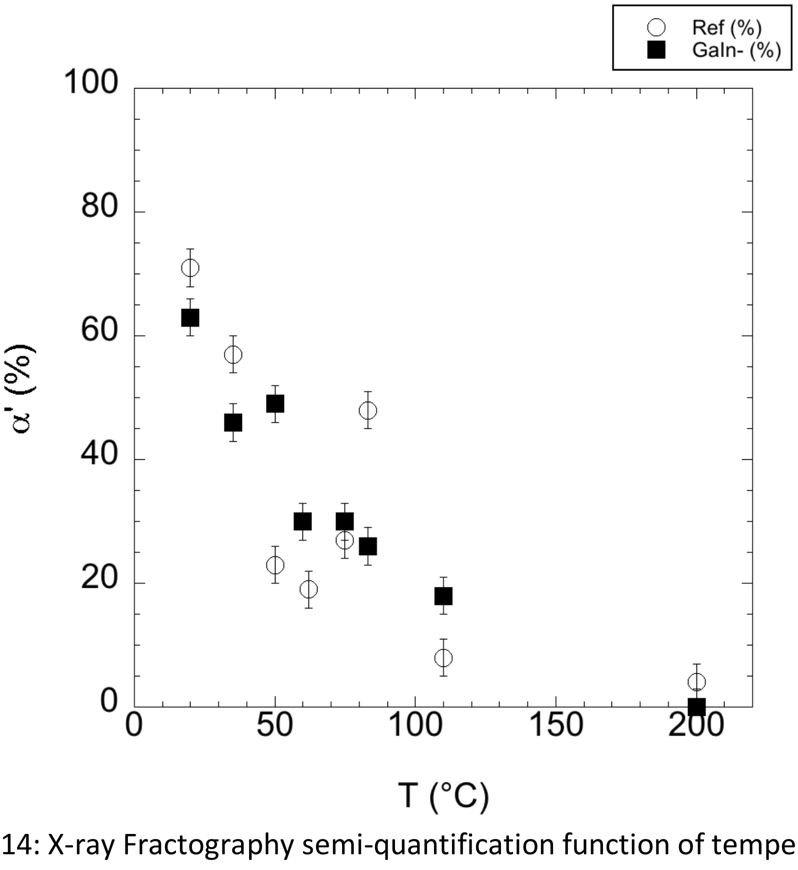

Figure 14: X-ray Fractography semi-quantification function of temperature

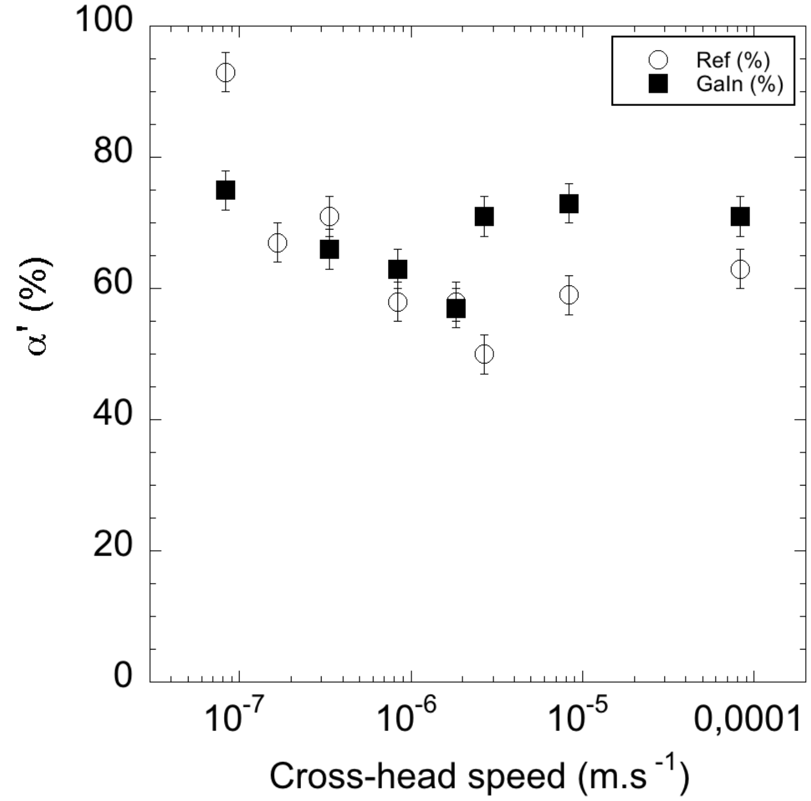

Figure 15: X-ray Fractography semi-quantification function of cross-head speed

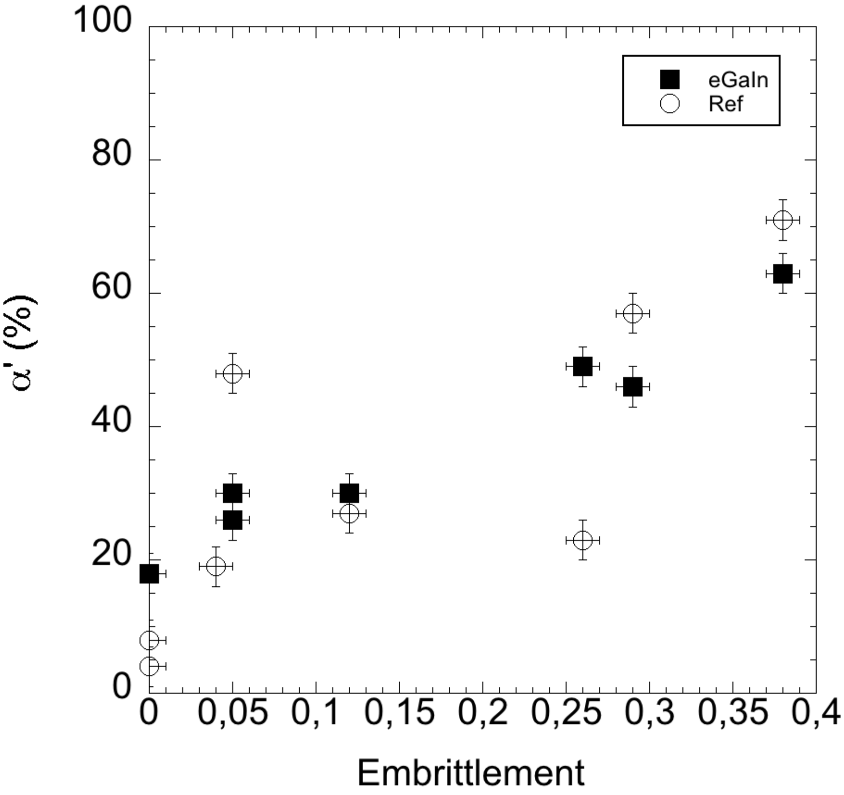

Figure 16: Correlation between degree of embrittlement and α' phase fraction for GaIn tested samples with varying temperatures [RT,110°C]